JPET Fast Forward. Published on June 16, 2020 as DOI: 10.1124/jpet.120.000009
This article has not been copyedited and formatted. The final version may differ from this version.

Voltage-Dependent Anion Channels Influence Cytotoxicity of ME-344, a Therapeutic Isoflavone

Leilei Zhang[1], Danyelle M. Townsend[2], Morgan Morris[1], Eduardo N. Maldonado[1], Yu-Lin Jiang[1], Ann-Marie Broome[1], Jennifer R. Bethard[1], Lauren E. Ball[1], Kenneth D. Tew[1*].

[1]Department of Cell and Molecular Pharmacology and Experimental Therapeutics, Medical University of South Carolina, 70 President St., DD410, Charleston, SC 29425, USA.

[2]Department of Pharmaceutical and Biomedical Sciences, Medical University of South Carolina, 274 Calhoun Street MSC 141, Charleston, S.C. 29425-1410, USA.

Downloaded from jpet.aspetjournals.org at ASPET Journals on April 20, 2024

JPET Fast Forward. Published on June 16, 2020 as DOI: 10.1124/jpet.120.000009
This article has not been copyedited and formatted. The final version may differ from this version.

Running title: VDAC influence on isoflavone pharmacology

[*]**Corresponding author:** Department of Cell and Molecular Pharmacology and Experimental Therapeutics, Medical University of South Carolina, 70 President St., DD410, Charleston, SC 29425, USA.

E-mail: tewk@musc.edu Tel. 843-792-2514; Fax. 843-792-2475

Number of text pages: 37

Number of tables: 0

Number of figures: 9

Number of references: 62

Number of words in the Abstract: 159

Number of words in the Introduction: 669

Number of words in the Discussion: 849

List of abbreviations:

ANT, adenine nucleotide translocase; Cyp-D, cyclophilin D; Cyt c, cytochrome c; Cyto, cytosol; ER, endoplasmic reticulum; HO-1, heme oxygenase 1; JC-1, 5,5',6,6'-tetrachloro-1,1',3,3'- tetra-ethylbenzimidazolylcarbocyanine iodide; Mito, mitochondria; MMP, mitochondrial membrane potential; MPT, mitochondrial permeability transition; PTP, permeability transition pore; ROS, reactive oxygen species; TMRM,

Downloaded from jpet.aspetjournals.org at ASPET Journals on April 20, 2024

JPET Fast Forward. Published on June 16, 2020 as DOI: 10.1124/jpet.120.000009
This article has not been copyedited and formatted. The final version may differ from this version.

tetramethylrhodamine methylester; VDAC, voltage-dependent anion channels.

Section Recommendation: Cellular and Molecular

Downloaded from jpet.aspetjournals.org at ASPET Journals on April 20, 2024

JPET Fast Forward. Published on June 16, 2020 as DOI: 10.1124/jpet.120.000009
This article has not been copyedited and formatted. The final version may differ from this version.

Abstract

ME-344 is a second generation cytotoxic isoflavone with anticancer activity promulgated through interference with mitochondrial functions. Using a click chemistry version of the drug together with affinity enriched mass spectrometry, voltage-dependent anion channels 1 and 2 (VDAC1, 2) were identified as drug targets. To determine the importance of VDAC1 or 2 to cytotoxicity we used lung cancer cells either sensitive (H460) or intrinsically resistant (H596) to the drug. In H460 cells, depletion of VDAC1 and VDAC2 by siRNA impacted ME-344 effects by: diminishing generation of reactive oxygen species (ROS); preventing mitochondrial membrane potential ($\Delta\Psi_m$) dissipation; moderating ME-344-induced cytotoxicity and mitochondrial mediated apoptosis. Mechanistically, VDAC1 and VDAC2 knockdown prevented ME-344-induced apoptosis by inhibiting Bax mitochondrial translocation and cytochrome c release as well as apoptosis in these H460 cells. We conclude that VDAC1 and 2, as mediators of the response to oxidative stress, have roles in modulating ROS generation, Bax translocation and cytochrome c release during mitochondrial-mediated apoptosis caused by ME-344.

Significance Statement

Dissecting preclinical drug mechanisms are of significance in development of a drug towards eventual FDA approval.

Downloaded from jpet.aspetjournals.org at ASPET Journals on April 20, 2024

JPET Fast Forward. Published on June 16, 2020 as DOI: 10.1124/jpet.120.000009
This article has not been copyedited and formatted. The final version may differ from this version.

Introduction

ME-344 as a synthetic isoflavone analogue of phenoxodiol with structural similarities to genestein, is currently in clinical trial in cancer patients (Bendell et al., 2015) (Diamond et al., 2017). One requirement towards attaining regulatory approval for the drug is to define its mechanism of action. Presently, it is apparent that mitochondria are directly impacted by drug treatment, but more than one molecular target has been identified. Possible interactive promiscuity is exemplified by reports that the drug induced inhibition of respiratory complexes (Alvero et al., 2011; Lim et al., 2015; Manevich et al., 2016; Navarro et al., 2016), and translocation of heme oxygenase 1 (HO-1) from rough endoplasmic reticulum to mitochondria (Manevich et al., 2016). In addition, ME-344 also causes increased mitochondrial ROS production, Bax mediated loss of mitochondrial membrane potential ($\Delta\Psi_m$) (Alvero et al., 2011; Zhang et al., 2019c), and inhibition of mitochondrial permeability transition (MPT; (Alvero et al., 2009)((Zhang et al., 2019c)). MPT is mediated through the opening/closing of a supramolecular complex permeability transition pore (PTP) between the inner and outer mitochondrial membranes. The molecular entities of the MPT pore are still debated, although hexokinase, voltage dependent anion channels (VDAC), adenine nucleotide translocase (ANT), and cyclophilin D (Cyp-D) have been proposed to be components of the pore (Zoratti et al., 2005; Brenner and Grimm, 2006). Bax, as a member of the Bcl-2 protein family, exists in equilibrium between mitochondria and cytosol (Schellenberg et al., 2013) and is also critical in maintaining MPT (Youle and Strasser, 2008).

Downloaded from jpet.aspetjournals.org at ASPET Journals on April 20, 2024

JPET Fast Forward. Published on June 16, 2020 as DOI: 10.1124/jpet.120.000009
This article has not been copyedited and formatted. The final version may differ from this version.

We recently used a click chemistry version of ME-344 and showed that it binds to, and inhibits, heme oxygenase 1 (HO-1). Proteomic analyses also indicated that VDAC 1 and 2 were binding targets (Zhang, 2019). VDAC, a highly conserved ~30 kDa protein with three isoforms in humans (VDAC1, 2 and 3), is the most abundant protein in the mitochondrial outer membrane (MOM). Respiratory substrates such as cytosolic ATP, ADP, and Pi entering mitochondria and mitochondrial ATP moving to the cytosol cross the MOM through VDAC (Colombini, 1989). The distribution of VDAC isoforms vary from cell to cell and from cancer cell line to cancer cell line but, in general, VDAC1 and VDAC2 are the most abundant isoforms. VDAC 1, the most studied isoform, has been proposed to play important roles in several physiological process including calcium signaling, regulation of cellular bioenergetics and ROS control. VDAC2, implicated in the regulation of apoptosis is also a major contributor of mitochondrial metabolism, whereas the minor isoform VDAC3, only recently has been shown to be a pore forming channel (De Pinto et al., 2010; McCommis and Baines, 2012; Maldonado et al., 2013b; Okazaki et al., 2015; Reina et al., 2016). Accumulating evidence indicates that VDAC play a role in determining cell survival (Rostovtseva and Colombini, 1996; Hodge and Colombini, 1997; Gincel et al., 2001) or apoptosis (Baek et al., 1997; Ding et al., 2001; Bae et al., 2003; Godbole et al., 2003; Zaid et al., 2005). Perhaps related to their interaction with the Bcl-2 family member Bax, VDAC1 and 2 have been implicated in regulation of apoptosis (Ma et al., 2014; Caterino et al., 2017). Silencing of VDAC1 or VDAC2 effectively prevents the association of Bcl-2 protein with mitochondria and inhibits Bax function and apoptosis induced by

Downloaded from jpet.aspetjournals.org at ASPET Journals on April 20, 2024

JPET Fast Forward. Published on June 16, 2020 as DOI: 10.1124/jpet.120.000009
This article has not been copyedited and formatted. The final version may differ from this version.

anti-cancer drugs (Tajeddine et al., 2008; Yuan et al., 2008; Chin et al., 2018; Dadsena et al., 2019a; Dadsena et al., 2019b).

It has been recently proposed that VDAC operates as a switch for global control of mitochondrial metabolism in cancer cells. Moreover, small molecules that cause VDAC opening increase mitochondrial metabolism and generation of reactive oxygen species (ROS) and decrease levels of enhanced glycolysis, acting as anti-Warburg compounds (Maldonado, 2017; Maldonado & Fang, 2018; DeHart et al., 2018; Heslop et al. 2020).

Since our previous click chemistry/proteomics analysis showed that ME-344 binds to VDAC1 and VDAC2, we undertook the present studies, focussing on these two isoforms to determine their relevance in drug response patterns in lung cancer cell lines that are either intrinsically sensitive or resistant to ME-344.

Downloaded from jpet.aspetjournals.org at ASPET Journals on April 20, 2024

JPET Fast Forward. Published on June 16, 2020 as DOI: 10.1124/jpet.120.000009
This article has not been copyedited and formatted. The final version may differ from this version.

Materials and Methods

Cell lines

H460 large cell lung cancer cells were from the National Cancer Institute (Frederick, MD) and H596 adenosquamous lung carcinoma cells were from ATCC. Each were maintained in RPMI1640 medium (Corning, N.Y.) supplemented with 10% (v/v) FBS (Atlas), 100 U/mL penicillin and 100 mg/mL streptomycin and 2 mmol/L L-glutamine. Cell lines were authenticated as described previously (Zhang et al., 2019b).

Antibodies

The following antibodies were used for immunoblots: Mouse monoclonal anti-ATP5A (ab110273) is from Abcam, Cambridge, MA. Mouse monoclonal anti-cytochrome c is from R&D SYSTEMS, Minneapolis, MN. Mouse monoclonal anti-Bax (B9054) and mouse monoclonal anti-β-actin are from Sigma, St. Louis, MO. IRDye 800CW Goat anti-Mouse immunoglobulin G (IgG), IRDye 800CW Goat anti-rabbit IgG, IRDye 680RD Goat anti-mouse IgG, and IRDye 680RD Goat anti-Rabbit IgG are all from LI-COR, Lincoln, NE.

Trypan blue assay

To determine the cell viability by vital dye exclusion tests, 20 µL of cell suspension were mixed with 20 µL of 0.4% trypan blue solution (Sigma-Aldrich) for 5 min. The number of viable cells were counted using a haemocytometer. Each experiment was carried out a minimum of three independent times. Means and standard deviations

Downloaded from jpet.aspetjournals.org at ASPET Journals on April 20, 2024

JPET Fast Forward. Published on June 16, 2020 as DOI: 10.1124/jpet.120.000009
This article has not been copyedited and formatted. The final version may differ from this version.

were calculated for each subculture.

ROS detection

ROS detection was performed as previously described (Zhang et al., 2019b). Cells were treated with 1 mmol/L 2',7' dichlorodihydrofluorescein diacetate (CM-H_2DCFDA; Thermo Fisher Scientific) for 45 minutes, followed by 2 times washes with PBS. The reduced CM-H_2DCFDA can be oxidized and converted into fluorescent 2', 7'-dichlorofluorescein (DCF) by intracellular ROS. The fluorescent signals were detected by flow cytometer (FCM, Beckman Coulter). Totally 10,000 cells were analyzed per sample.

siRNA Treatment

Cells grown to 70–80% confluence were transfected with siRNA (50 nM) targeting VDAC1, VDAC2, and VDAC3 or control non-target siRNA (Ambion, Austin, TX). Non-target siRNA was Silencer Select Negative Control #1 siRNA (Catalogue #4390844). siRNAs for VDAC1, VDAC2, and VDAC3 were Silencer Select siRNAs: VDAC1, Catalogue #4390824, ID: s14769; VDAC2, Catalogue #4392420, ID:s14771; and VDAC3, Catalogue #4392420, ID:s230730. siRNAs were reverse transfected using lipofectamine RNAiMAX Transfection Reagent according to the manufacturer's instructions (Invitrogen, Carlsbad, CA).

RNA isolation and quantitative real-time reverse transcription-PCR

RNA isolation and real-time PCR were performed as described previously (Zhang et

Downloaded from jpet.aspetjournals.org at ASPET Journals on April 20, 2024

JPET Fast Forward. Published on June 16, 2020 as DOI: 10.1124/jpet.120.000009
This article has not been copyedited and formatted. The final version may differ from this version.

al., 2019b). Total RNA was prepared using the Isolate II RNA Mini Kit (Bioline USA, Inc.) and cDNA then synthesized with the iScript cDNA Synthesis Kit (Bio-Rad). Subsequently, quantification of gene expression was performed in duplicate using iQ SYBR Green Supermix (Bio- Rad) with detection on a MyiQ Real-Time PCR System (Bio-Rad). The reaction cycles used were 95˚C for 5 minutes, 40 cycles at 95˚C for 15 seconds and 58˚C for 1 minute followed by melt curve analysis. Relative gene expression quantification was based on the comparative threshold cycle (CT) method (2^DDCt) with normalization of the raw data to the housekeeping gene (18S rRNA).

Loading of tetramethylrhodamine methylester (TMRM) and laser scanning confocal microscopy

H460 (drug sensitive) and H596 (drug resistant) cells plated in MatTek dishes were loaded with 200 nM TMRM for 30 min in modified Hank´s balanced salt solution (HBSS) containing (in mM): NaCl 137, Na_2HPO_4 0.35, KCl 5.4, KH_2PO_4 1, $MgSO_4$ 0.81, $CaCl_2$ 0.95, glucose 5.5, $NaHCO_3$ 25 and HEPES 20, pH 7.4, or complete growth media. After the initial loading, cells were maintained in 50 nM TMRM to maintain the equilibrium of distribution (Lemasters and Ramshesh 2007). Cells incubated in modified HBSS in a humidified 5% CO_2/air at 37° C were imaged with a Zeiss LSM 880 NLO inverted laser scanning confocal microscope (Thornwood, NY) with a 63X 1.4 N.A. plan apochromat oil immersion lens. TMRM was excited at 561 nm and emission signal was detected with a Quasar multichannel spectral detector at 590–610 nm through a one Airy unit diameter pinhole. (Maldonado et al., 2013a).

Downloaded from jpet.aspetjournals.org at ASPET Journals on April 20, 2024

JPET Fast Forward. Published on June 16, 2020 as DOI: 10.1124/jpet.120.000009
This article has not been copyedited and formatted. The final version may differ from this version.

JC-1 staining

Cells were stained with the mitochondrial membrane potential sensitive probe, JC-1 (5,5',6,6'-tetrachloro-1,1',3,3'- tetra-ethylbenzimidazolylcarbocyanine iodide) (Invitrogen), at a final concentration of 2 µM in PBS for 15 min at 37°C. After two PBS washes (300×g, 5 min), labeled cells were observed with an Olympus FV10i laser scanning confocal. The aggregate red form of JC-1 has absorption/emission maxima of 585/590 nm, while the green monomeric form is 510/527 nm. Images acquired from confocal microscopy were measured and calculated for mean fluorescence intensities (MFI) using ImageJ software version 1.41 (Rasband, W.S., ImageJ, U. S. National Institutes of Health, Bethesda, Maryland, USA). For flow cytometry, JC-1 aggregates were measured in the FL-2 channel, and JC-1 monomer in the FL-1 channel. FACS data were analyzed by CytExpert.

Apoptosis assay

Annexin V and PI staining were performed according to the manufacturer's instructions (BD Pharmingen, 556547,). Cells were washed twice with cold PBS and then resuspended in 1X Binding Buffer at a concentration of 1 x 10^6 cells/ml. 100 µl of the solution (1 x 10^5 cells) was transferred to a 5 ml culture tube and 5 µl of FITC Annexin V and 5 µl PI added. Cells were vortexed and incubated for 15 min at 25°C in the dark. 400 µl of 1X Binding Buffer was added to each tube and subject to flow cytometry within 1 hr.

Purification of mitochondria and cytosol

Downloaded from jpet.aspetjournals.org at ASPET Journals on April 20, 2024

JPET Fast Forward. Published on June 16, 2020 as DOI: 10.1124/jpet.120.000009
This article has not been copyedited and formatted. The final version may differ from this version.

Mitochondria and cytosol fractions were isolated as previously described (Wettmarshausen and Perocchi, 2017). Purities of cell fractions were determined by immunoblotting against β-actin (cytosol marker), ATP5A (mitochondrial marker) and SERCA (endoplasmic reticulum (ER) marker).

Immunoblotting

Immunoblotting was performed as previously described (Zhang et al., 2019b). Total soluble protein was quantitated by bicinchoninic acid protein assay (Pierce). Mitochondria and cytosol fractions were resolved in an SDS-loading buffer [80 mmol/L Tris-HCl, pH 6.8, 2% SDS, 10% glycerol, 0.02% bromophenol blue, 5 mmol/L tris (2-carboxyethyl) phosphine] and heated at 95°C for 5 minutes. Equal amounts (50 ug) of protein were electrophoretically separated by SDS PAGE (Bio-Rad) and transferred onto low fluorescent polyvinylidene fluoride membranes (Millipore) by the Trans-Blot Turbo Transfer System (Bio-Rad). PVDF or nitrocellulose membranes were incubated in the Odyssey blocking buffer (LI-COR) for 1 hour to reduce nonspecific binding and then probed with appropriate primary antibodies at 4°C overnight. Immunoblots were then developed with infrared (IR) fluorescence IRDye secondary antibodies (LI-COR) at a dilution of 1:15,000, imaged with a 2-channel (red and green) IR fluorescent Odyssey CLx imaging system (LI-COR) and quantified with ImageJ software (FIJI).

Click Chemistry and Affinity Enrichment Mass Spectrometry

Click chemistry and LC-MS/MS were performed as previously described (Zhang et al., 2019b). However, while the previous analysis focused only on drug-enriched proteins

Downloaded from jpet.aspetjournals.org at ASPET Journals on April 20, 2024

JPET Fast Forward. Published on June 16, 2020 as DOI: 10.1124/jpet.120.000009
This article has not been copyedited and formatted. The final version may differ from this version.

of 25-50 kDa, the present study was expanded. All proteins enriched by ME-344 beads (or negative controls) were fractionated into six gel bands before in-gel digestion and analyzed by LC-MS/MS. Quantitative results were extracted and analyzed using MaxQaunt and Perseus. Proteins were filtered to retain only those quantified in duplicate ME-344 enrichments and missing values in the control enrichment were recorded as previously described (Zhang et al., 2019b)

Protein interaction and annotation networks were generated using a web-based tool, NDEx (Pratt et al., 2015) (Pillich et al., 2017) (Pratt et al., 2017). Protein interactions associated with enriched proteins were extracted from multiple protein interaction databases accessible in NDEx (BIOGRID, String, HumanNet, HIPPIE) and merged and visualized with Cytoscape 3.8.0 (Shannon et al., 2003) (Otasek et al., 2019). Annotated gene-pathway relationships of VDAC1 and VDAC2 curated in the Comparative Toxicogenomics Database (Davis et al., 2019) were accessed through NDEx Integrated Query and visualized with Cytoscape.

Statistical analysis

All measurements were collected from 3 independent experiments. Statistical analysis was performed using GraphPad Prism 6.0 and Microsoft Excel. Significant differences were determined using 2 tailed t tests. The results are expressed as the means ± SD. Significance levels were established at a level of $P < 0.05$.

Downloaded from jpet.aspetjournals.org at ASPET Journals on April 20, 2024

JPET Fast Forward. Published on June 16, 2020 as DOI: 10.1124/jpet.120.000009
This article has not been copyedited and formatted. The final version may differ from this version.

Results

ME-344 binds directly to VDAC 1 and 2

Using a monopropargylated derivative of ME-344 (M2F) (Supplemental Fig. S1) with azide agarose resin (Zhang et al., 2019b) we identified protein binding via affinity enrichment-mass spectrometry. Our previous study focused on a single, differentially stained gel band, whereas the analysis described in this report was designed to discern differentially enriched proteins from full protein profiles. The relative abundance of proteins enriched by M2F conjugated beads was compared with control resin, measured by label free proteomics (Supplemental Table S1). Twelve proteins were enriched by M2F beads, determined by a >2.5 $\log_2$ fold change compared to control beads. These included VDAC1 and 2, enriched by 3.55- and 3.25-$\log_2$ fold respectively (Fig. 1A). Enriched proteins were queried for known interactions and the resulting protein interaction networks were uploaded and merged with the drug-protein interaction network in Cytoscape. This analysis revealed VDAC 1 and 2 were central to the network, interacting with 5 of the other enriched proteins, indicating direct binding of the drug to VDAC and enrichment of VDAC binding proteins (Fig. 1B). Functional annotations associated with VDAC 1 and 2 are shown in Fig. 1C.

VDAC expression, ROS production and drug response.

As assessed by qPCR, all three VDAC isoforms were expressed in both H460 and H596 cells. Proportionally, VDAC2 (48% and 60%) was the most abundant, followed

Downloaded from jpet.aspetjournals.org at ASPET Journals on April 20, 2024

JPET Fast Forward. Published on June 16, 2020 as DOI: 10.1124/jpet.120.000009
This article has not been copyedited and formatted. The final version may differ from this version.

by VDAC1 (30% and 27%) and VDAC3 (22% and 13% respectively; Fig. 2A). We previously established that H460 cells are sensitive and H596 intrinsically resistant to ME-344 and found no significant difference of basal protein levels of VDAC1 and VDAC2 in H460 and H596 cells. However, when challenged with ME-344, fold changes of VDAC1 and VDAC2 were both more pronounced in H460 cells than H596 cells. Interestingly, MRC-5, normal lung fibroblasts cells, was more closely aligned to the resistant than sensitive cells in the expression of VDAC1 and VDAC2 after ME-344 treatment (Supplemental Fig. S2) (Zhang et al., 2019b). Isoform-specific siRNAs selectively inhibited expression of VDAC1, 2 and 3 respectively. siRNAs treatment decreased both mRNA and protein expression by approximately 90% for each isoform, without causing compensatory increases on expression of the other isoforms (Fig. 2B,C). Response to ME-344 (trypan blue assay), and ROS production were determined after individual knockdown of each isoform in comparison with non-target treated cells. The cell viabilities were shown in Fig. 2D,E and Supplemental Table S2. The IC_{50}s for ME-344 in siVDAC1 and siVDAC2 knockdown H460 cells increased by 46.7% and 37.4% respectively compared with non-target siRNAs. There were no significant changes of IC_{50}s in H596 cells. Knockdown of VDAC 1 or 2 slightly decreased basal ROS levels, while VDAC 3 knockdown increased basal ROS levels in H460 cells (Fig. 2F,G). ROS production of H596 cells was unaffected (Fig. 2H,I). Since ROS can induce mitochondrial permeability transition pore opening, we measured how ROS levels were influenced by VDAC knockdown. Reduced VDAC 1 or 2 levels resulted in decreased ROS generation, while knockdown of VDAC 3

Downloaded from jpet.aspetjournals.org at ASPET Journals on April 20, 2024

JPET Fast Forward. Published on June 16, 2020 as DOI: 10.1124/jpet.120.000009
This article has not been copyedited and formatted. The final version may differ from this version.

increased ROS production induced by ME-344 compared to non-target siRNA (Fig. 3A-H).

Knockdown of VDAC 1 or 2 decreased apoptosis induced by ME-344 in H460 cells. The respective contributions of early (Annexin V-FITC positive, PI negative) and late stage apoptosis (both Annexin V-FITC and PI positive) were measured in H460 cells following ME-344. The results showed that apoptosis rates increased in a dose-dependent manner in comparison to untreated cells. H596 cells were unaffected by similar drug concentrations (Fig. 4A-D). Knockdown of either VDAC 1 or 2 did however decrease the levels of apoptosis induced by ME-344 compared to non-target siRNA (Fig. 5A-L).

ME-344 affects on mitochondrial membrane potential.

Loss of $\Delta\Psi_m$, is an indicator of mitochondrial dysfunction that, in some cases, triggers the release of cytochrome c from mitochondria to the cytoplasm, and activate the apoptotic caspase cascade. Previously, we showed that ME-344-induced apoptosis by activation of caspase-3, that led to the cleavage of PARP (Zhang et al., 2019a). In this regard, ME-344 treatment decreased $\Delta\Psi_m$ in a dose dependent manner in H460 cells as shown by confocal imaging of JC-1 fluorescence (Fig. 6A,B) and flow cytometry (Fig. 6C,D). These effects were not apparent for the resistant H596 cells (Fig. 6E-H).

To assess the time at which $\Delta\Psi_m$ began to change in H460 and H596 cells, we loaded cells with the potential-indicating fluorophore TMRM and subsequently imaged with

Downloaded from jpet.aspetjournals.org at ASPET Journals on April 20, 2024

JPET Fast Forward. Published on June 16, 2020 as DOI: 10.1124/jpet.120.000009
This article has not been copyedited and formatted. The final version may differ from this version.

confocal microscopy. Vehicle or ME-344 treated cells in the same fields were followed for 3 h. ME-344 induced significant depolarization of $\Delta\Psi_m$ within 15 min in H460 cells (approximately 40%) and by more than 60% at the end of the 3-h treatment (Fig. 7A,B). No significant depolarization was induced by ME-344 in H596 cells (Fig. 7C,D). These data were confirmed using flow cytometry (Fig. 7E-H). To assess the impact of silencing VDAC on $\Delta\Psi_m$, both H460 and H596 cells were transfected with either non-target or VDAC 1, 2, 3 siRNAs and subsequently loaded with TMRM and imaged by confocal microscopy. In non-target siRNA H460 cells, mitochondria expressed strong labeling with TMRM (Fig. 8A). Knockdown of VDAC isoforms 1, 2, and 3 decreased mitochondrial TMRM fluorescence by 19, 18, and 26%, respectively. The most significant decrease of $\Delta\Psi_m$ occurred after knockdown of VDAC3, the least abundant isoform (Fig. 8B). ME-344 reduced the TMRM fluorescence in mitochondria, indicated by reduction in $\Delta\Psi_m$ in H460 cells (Fig. 8A,C). This drug induced dissipation of $\Delta\Psi$m was diminished by knockdown of either VDAC 1 or 2 in H460 cells (Fig. 8A,C).

VDAC1 and 2 are required for Bax to mediate ME-344-induced apoptosis in H460 cells.

Bax translocation from cytosol to mitochondria induces cytochrome c release, followed by caspase activation of apoptosis (Tang et al., 2006; George et al., 2010; Wang et al., 2013). To determine whether VDACs influence this process, Bax and cytochrome c levels were determined in mitochondria and cytosol in both H460 and

Downloaded from jpet.aspetjournals.org at ASPET Journals on April 20, 2024

JPET Fast Forward. Published on June 16, 2020 as DOI: 10.1124/jpet.120.000009
This article has not been copyedited and formatted. The final version may differ from this version.

H596 cells. ME-344 treatments of H460 with VDAC1 or 2 knockdown decreased both Bax translocation from cytosol to mitochondria and release of cytochrome c. These effects were not found in either VDAC3 or non-target knockdowns (Fig. 9A,B). Bax translocation and cytochrome c release were not affected in transfected H596 cells (Fig. 9C,D). Taken together, these results showed that VDAC1 and 2, but not 3, influenced ME-344 mediated Bax translocation mediated apoptosis in H460 cells.

Downloaded from jpet.aspetjournals.org at ASPET Journals on April 20, 2024

JPET Fast Forward. Published on June 16, 2020 as DOI: 10.1124/jpet.120.000009
This article has not been copyedited and formatted. The final version may differ from this version.

Discussion

ME-344 has progressed into Phase I/II clinical trials (Bendell et al., 2015; Miguel Quintela-Fandino, 2018). An overview of preclinical studies indicates that the drug exerts its cytotoxic effects by targetting mitochondria in a number of different cancer types, including lung cancers (Zhang et al., 2019c). The observation that ME-344 can inhibit respiratory complexes with subsequent dysregulation of cellular ROS levels provided impetus for us to consider HO-1 as a potential drug target (Alvero et al., 2011; Lim et al., 2015; Manevich et al., 2016; Navarro et al., 2016). We used click chemistry approaches to confirm that HO-1 is a direct target for ME-344 binding, and found that it: time-dependently inhibited activity of HO-1; bound to and altered HO-1 protein structure; induced HO-1 translocation from ER to mitochondria. Its inhibition disrupted redox homeostasis leading to mitochodrial-mediated apoptosis (Zhang et al., 2019b). Our proteomic analysis of the click chemistry results also identified other mitochondrial proteins that were plausibly affected by ME-344 treatments. Amongst these, VDAC1 and VDAC2 were implicated (Zhang et al., 2019b). In light of the role of VDACs in response to oxidative stress (Noskov et al., 2016), this observation provided a platform for the present study, designed to interrogate whether drug effects on these mitochondrial membrane proteins were associated with drug cytotoxicity.

The present results showed that VDAC1 and 2 were enriched by 3.55- and 3.25-$\log_2$ fold transformed intensities of drug binding when compared with their respective controls (Fig. 1). By using lung cancer cells either intrinsically sensitive (H460) or

Downloaded from jpet.aspetjournals.org at ASPET Journals on April 20, 2024

JPET Fast Forward. Published on June 16, 2020 as DOI: 10.1124/jpet.120.000009
This article has not been copyedited and formatted. The final version may differ from this version.

resistant (H596) to the drug, and employing siRNA to deplete each individual VDAC isoform, we were able to consider their relevance to drug effects. Our results indicated that genetic manipulation of either VDAC1 or 2 expression did influence drug sensitivity, intracellular ROS levels and induction of apoptosis. Knockdown of either VDAC 1 or 2 reduced intracellular ROS levels and made H460 cells less susceptible to ME-344 cytotoxicity. These observations are consistent with other reports showing that VDAC1 silencing lowered both ROS and cell death induced by either selenite (Tomasello et al., 2009) or cisplatin (Tajeddine et al., 2008). Contextually, ROS are known to initiate mitochondrial permeability transition pore (mPTP) opening in mammalian cells (Zoratti and Szabo, 1994). As one of the major putative components of mPTP, VDACs are localized in the outer mitochondrial membrane (OMM), and are critical components to the formation of this pore (Vianello et al., 2012). Under physiological conditions, VDACs facilitate metabolite exchange between mitochondria and cytosol; increase conductance, linked to mPTP opening; dissipate $\Delta\Psi_m$ and eventual cytochrome c release, characteristics of the early stages of ME-344 toxicity, leading to cell death (Shimizu et al., 1999; Tsujimoto and Shimizu, 2000). Our data show that ME-344 induced loss of $\Delta\Psi_m$ in both non-target and siVDAC3 H460 cells, but no $\Delta\Psi_m$ changes were detected in siVDAC1 or siVDAC2 treated H460 cells. VDAC1 and 2 knockdown not only prevented the decrease in $\Delta\Psi_m$ following ME-344, but also prevented Bax translocation and cytochrome c release. Bax, as a proapoptotic member of the Bcl-2 family of proteins, is a critical contributor to mitochondrial mediated apoptosis pathways. Under non-stress conditions, Bax

Downloaded from jpet.aspetjournals.org at ASPET Journals on April 20, 2024

JPET Fast Forward. Published on June 16, 2020 as DOI: 10.1124/jpet.120.000009
This article has not been copyedited and formatted. The final version may differ from this version.

locates predominantly in the cytosol, but various exogenous stresses can cause its translocation to mitochondria as a prelude to apoptosis (Haneef et al., 2012; Li et al., 2013; Wang et al., 2013). Depletion of VDAC1 and 2 prevented both ME-344-induced Bax translocation from cytosol to mitochondria and cytochrome c release from mitochondria to cytosol. These results indicate that in H460 cells the apoptosis caused by ME-344 is contingent upon VDAC1 and 2 and disabling them can contribute to enhanced ROS, contributing to the cytoxic properties of ME-344.

There are other drugs that bind to VDAC2 and VDAC3. Erastin causes oxidative stress and mitochondrial dysfunction (Yagoda et al., 2007) through iron accumulation, ROS production resulting in ferroptosis, (Dixon et al., 2012) reversible by iron chelation or antioxidants (Xu et al., 2019). Since HO-1 initiates catabolism of heme and increases cellular iron levels (Suttner and Dennery, 1999) ME-344 binding to both HO-1 and VDACs may imply that it shares some properties with erastin. Interactions between VDAC and mitoNEET, an integral outer mitochondrial iron sulfur cluster protein that can regulate VDAC transport in cancer cells, can be disrupted by agents (e.g. pioglitazone) that target VDAC and is redox dependent (Paddock et al., 2007; Lipper et al., 2019). ME-344 appears to have promiscuous affinity for a number of mitochondrial proteins, inducing apoptosis by disrupting mitochondrial homeostasis, promoting ROS production, loss of $\Delta\Psi_m$, Bax translocation and cytochrome c release. We would argue that these outcomes are downstream of drug binding to VDAC's and HO-1 (Zhang, 2019), each of which disrupt the cell's capacity to maintain redox homeostasis. In this instance, knockdown of VDACs diminished the effects that

Downloaded from jpet.aspetjournals.org at ASPET Journals on April 20, 2024

JPET Fast Forward. Published on June 16, 2020 as DOI: 10.1124/jpet.120.000009
This article has not been copyedited and formatted. The final version may differ from this version.

ME-344 triggered in H460 cells, indicating cellular expression levels of VDAC1 and VDAC2 are essential regulators of apoptosis induction by ME-344, and perhaps some of the other VDAC1 targeting agents discussed elsewhere (Ben-Hail et al., 2016). This component of the drug's mechanism will be of consequence in the design of combinatorial therapeutic strategies in managing, for example, lung cancer.

Downloaded from jpet.aspetjournals.org at ASPET Journals on April 20, 2024

JPET Fast Forward. Published on June 16, 2020 as DOI: 10.1124/jpet.120.000009
This article has not been copyedited and formatted. The final version may differ from this version.

Acknowledgements

The authors thank Jennifer Bethard (Mass Spectrometry Facility, Medical University of South Carolina) for her help in providing previous proteomic analysis.

Authorship contributions:

Participated in research design: K.D.T and D.M.T

Conducted experiments: L.Z, J.R.B and Y.J

Contributed new reagents or analytic tools: M.M

Performed data analysis: L.Z, L.E.B and A.B

Wrote or contributed to the writing of the manuscript: K.D.T, E.M and L.Z

Downloaded from jpet.aspetjournals.org at ASPET Journals on April 20, 2024

JPET Fast Forward. Published on June 16, 2020 as DOI: 10.1124/jpet.120.000009
This article has not been copyedited and formatted. The final version may differ from this version.

References

Alvero AB, Montagna MK, Chen R, Kim KH, Kyungjin K, Visintin I, Fu HH, Brown D and Mor G (2009) NV-128, a novel isoflavone derivative, induces caspase-independent cell death through the Akt/mammalian target of rapamycin pathway. *Cancer* **115**:3204-3216.

Alvero AB, Montagna MK, Holmberg JC, Craveiro V, Brown D and Mor G (2011) Targeting the mitochondria activates two independent cell death pathways in ovarian cancer stem cells. *Mol Cancer Ther* **10**:1385-1393.

Bae JH, Park JW and Kwon TK (2003) Ruthenium red, inhibitor of mitochondrial Ca2+ uniporter, inhibits curcumin-induced apoptosis via the prevention of intracellular Ca2+ depletion and cytochrome c release. *Biochem Biophys Res Commun* **303**:1073-1079.

Baek JH, Lee YS, Kang CM, Kim JA, Kwon KS, Son HC and Kim KW (1997) Intracellular Ca2+ release mediates ursolic acid-induced apoptosis in human leukemic HL-60 cells. *Int J Cancer* **73**:725-728.

Ben-Hail D, Begas-Shvartz R, Shalev M, Shteinfer-Kuzmine A, Gruzman A, Reina S, De Pinto V and Shoshan-Barmatz V (2016) Novel Compounds Targeting the Mitochondrial Protein VDAC1 Inhibit Apoptosis and Protect against Mitochondrial Dysfunction. *J Biol Chem* **291**:24986-25003.

Bendell JC, Patel MR, Infante JR, Kurkjian CD, Jones SF, Pant S, Burris HA, 3rd, Moreno O, Esquibel V, Levin W and Moore KN (2015) Phase 1, open-label, dose escalation, safety, and pharmacokinetics study of ME-344 as a single agent in patients with

Downloaded from jpet.aspetjournals.org at ASPET Journals on April 20, 2024

JPET Fast Forward. Published on June 16, 2020 as DOI: 10.1124/jpet.120.000009
This article has not been copyedited and formatted. The final version may differ from this version.

refractory solid tumors. *Cancer* **121**:1056-1063.

Brenner C and Grimm S (2006) The permeability transition pore complex in cancer cell death. *Oncogene* **25**:4744-4756.

Caterino M, Ruoppolo M, Mandola A, Costanzo M, Orru S and Imperlini E (2017) Protein-protein interaction networks as a new perspective to evaluate distinct functional roles of voltage-dependent anion channel isoforms. *Mol Biosyst* **13**:2466-2476.

Chin HS, Li MX, Tan IKL, Ninnis RL, Reljic B, Scicluna K, Dagley LF, Sandow JJ, Kelly GL, Samson AL, Chappaz S, Khaw SL, Chang C, Morokoff A, Brinkmann K, Webb A, Hockings C, Hall CM, Kueh AJ, Ryan MT, Kluck RM, Bouillet P, Herold MJ, Gray DHD, Huang DCS, van Delft MF and Dewson G (2018) VDAC2 enables BAX to mediate apoptosis and limit tumor development. *Nat Commun* **9**:4976.

Colombini M (1989) Voltage gating in the mitochondrial channel, VDAC. *J Membr Biol* **111**:103-111.

Dadsena S, Bockelmann S, Mina JGM, Hassan DG, Korneev S, Razzera G, Jahn H, Niekamp P, Muller D, Schneider M, Tafesse FG, Marrink SJ, Melo MN and Holthuis JCM (2019a) Ceramides bind VDAC2 to trigger mitochondrial apoptosis. *Nat Commun* **10**:1832.

Dadsena S, Hassan DG and Holthuis JCM (2019b) Unraveling the molecular principles by which ceramides commit cells to death. *Cell Stress* **3**:280-283.

Davis AP, Grondin CJ, Johnson RJ, Sciaky D, McMorran R, Wiegers J, Wiegers TC and Mattingly CJ (2019) The Comparative Toxicogenomics Database: update 2019. *Nucleic Acids Res* **47**:D948-D954.

Downloaded from jpet.aspetjournals.org at ASPET Journals on April 20, 2024

JPET Fast Forward. Published on June 16, 2020 as DOI: 10.1124/jpet.120.000009
This article has not been copyedited and formatted. The final version may differ from this version.

De Pinto V, Guarino F, Guarnera A, Messina A, Reina S, Tomasello FM, Palermo V and Mazzoni C (2010) Characterization of human VDAC isoforms: a peculiar function for VDAC3? *Biochim Biophys Acta* **1797**:1268-1275.

Diamond JR, Goff B, Forster MD, Bendell JC, Britten CD, Gordon MS, Gabra H, Waterhouse DM, Poole M, Ross Camidge D, Hamilton E and Moore KM (2017) Phase Ib study of the mitochondrial inhibitor ME-344 plus topotecan in patients with previously treated, locally advanced or metastatic small cell lung, ovarian and cervical cancers. *Invest New Drugs*.

Ding WX, Shen HM and Ong CN (2001) Pivotal role of mitochondrial Ca(2+) in microcystin-induced mitochondrial permeability transition in rat hepatocytes. *Biochem Biophys Res Commun* **285**:1155-1161.

Dixon SJ, Lemberg KM, Lamprecht MR, Skouta R, Zaitsev EM, Gleason CE, Patel DN, Bauer AJ, Cantley AM, Yang WS, Morrison B, 3rd and Stockwell BR (2012) Ferroptosis: an iron-dependent form of nonapoptotic cell death. *Cell* **149**:1060-1072.

George NM, Targy N, Evans JJ, Zhang L and Luo X (2010) Bax contains two functional mitochondrial targeting sequences and translocates to mitochondria in a conformational change- and homo-oligomerization-driven process. *J Biol Chem* **285**:1384-1392.

Gincel D, Zaid H and Shoshan-Barmatz V (2001) Calcium binding and translocation by the voltage-dependent anion channel: a possible regulatory mechanism in mitochondrial function. *Biochem J* **358**:147-155.

Godbole A, Varghese J, Sarin A and Mathew MK (2003) VDAC is a conserved element of

Downloaded from jpet.aspetjournals.org at ASPET Journals on April 20, 2024

JPET Fast Forward. Published on June 16, 2020 as DOI: 10.1124/jpet.120.000009
This article has not been copyedited and formatted. The final version may differ from this version.

death pathways in plant and animal systems. *Biochim Biophys Acta* **1642**:87-96.

Haneef J, Parvathy M, Thankayyan RS, Sithul H and Sreeharshan S (2012) Bax translocation mediated mitochondrial apoptosis and caspase dependent photosensitizing effect of Ficus religiosa on cancer cells. *PLoS One* **7**:e40055.

Hodge T and Colombini M (1997) Regulation of metabolite flux through voltage-gating of VDAC channels. *J Membr Biol* **157**:271-279.

Li Z, Meng J, Xu TJ, Qin XY and Zhou XD (2013) Sodium selenite induces apoptosis in colon cancer cells via Bax-dependent mitochondrial pathway. *Eur Rev Med Pharmacol Sci* **17**:2166-2171.

Lim SC, Carey KT and McKenzie M (2015) Anti-cancer analogues ME-143 and ME-344 exert toxicity by directly inhibiting mitochondrial NADH: ubiquinone oxidoreductase (Complex I). *Am J Cancer Res* **5**:689-701.

Lipper CH, Stofleth JT, Bai F, Sohn YS, Roy S, Mittler R, Nechushtai R, Onuchic JN and Jennings PA (2019) Redox-dependent gating of VDAC by mitoNEET. *Proc Natl Acad Sci U S A* **116**:19924-19929.

Ma SB, Nguyen TN, Tan I, Ninnis R, Iyer S, Stroud DA, Menard M, Kluck RM, Ryan MT and Dewson G (2014) Bax targets mitochondria by distinct mechanisms before or during apoptotic cell death: a requirement for VDAC2 or Bak for efficient Bax apoptotic function. *Cell Death Differ* **21**:1925-1935.

Maldonado EN, Sheldon KL, DeHart DN, Patnaik J, Manevich Y, Townsend DM, Bezrukov SM, Rostovtseva TK and Lemasters JJ (2013a) Voltage-dependent anion channels modulate mitochondrial metabolism in cancer cells: regulation by free tubulin and

Downloaded from jpet.aspetjournals.org at ASPET Journals on April 20, 2024

JPET Fast Forward. Published on June 16, 2020 as DOI: 10.1124/jpet.120.000009
This article has not been copyedited and formatted. The final version may differ from this version.

erastin. *J Biol Chem* **288**:11920-11929.

Maldonado EN, Sheldon KL, DeHart DN, Patnaik J, Manevich Y, Townsend DM, Bezrukov SM, Rostovtseva TK and Lemasters JJ (2013b) Voltage-dependent anion channels modulate mitochondrial metabolism in cancer cells: regulation by free tubulin and erastin. *The Journal of biological chemistry* **288**:11920-11929.

Manevich Y, Reyes L, Britten CD, Townsend DM and Tew KD (2016) Redox Signaling and Bioenergetics Influence Lung Cancer Cell Line Sensitivity to the Isoflavone ME-344. *J Pharmacol Exp Ther* **358**:199-208.

McCommis KS and Baines CP (2012) The role of VDAC in cell death: friend or foe? *Biochim Biophys Acta* **1818**:1444-1450.

Miguel Quintela-Fandino JVA, Alfonso Cortes Salgado, Silvana Andrea Mouron, Juan Antonio Guerra, Mana Gion Cortes, Manuel Morente, Luis Manso (2018) Abrogation of resistance against bevacizumab (Bev) by mitochondrial inhibition: A phase 0 randomized trial of Bev plus ME344 or placebo in early HER2-negative breast cancer (HERNEBC). *J Clinical Oncology* **36**:abstract 2552.

Navarro P, Bueno MJ, Zagorac I, Mondejar T, Sanchez J, Mouron S, Munoz J, Gomez-Lopez G, Jimenez-Renard V, Mulero F, Chandel NS and Quintela-Fandino M (2016) Targeting Tumor Mitochondrial Metabolism Overcomes Resistance to Antiangiogenics. *Cell Rep* **15**:2705-2718.

Noskov SY, Rostovtseva TK, Chamberlin AC, Teijido O, Jiang W and Bezrukov SM (2016) Current state of theoretical and experimental studies of the voltage-dependent anion channel (VDAC). *Biochim Biophys Acta* **1858**:1778-1790.

Downloaded from jpet.aspetjournals.org at ASPET Journals on April 20, 2024

JPET Fast Forward. Published on June 16, 2020 as DOI: 10.1124/jpet.120.000009
This article has not been copyedited and formatted. The final version may differ from this version.

Okazaki M, Kurabayashi K, Asanuma M, Saito Y, Dodo K and Sodeoka M (2015) VDAC3 gating is activated by suppression of disulfide-bond formation between the N-terminal region and the bottom of the pore. *Biochim Biophys Acta* **1848**:3188-3196.

Otasek D, Morris JH, Boucas J, Pico AR and Demchak B (2019) Cytoscape Automation: empowering workflow-based network analysis. *Genome Biol* **20**:185.

Paddock ML, Wiley SE, Axelrod HL, Cohen AE, Roy M, Abresch EC, Capraro D, Murphy AN, Nechushtai R, Dixon JE and Jennings PA (2007) MitoNEET is a uniquely folded 2Fe 2S outer mitochondrial membrane protein stabilized by pioglitazone. *Proc Natl Acad Sci U S A* **104**:14342-14347.

Pillich RT, Chen J, Rynkov V, Welker D and Pratt D (2017) NDEx: A Community Resource for Sharing and Publishing of Biological Networks. *Methods Mol Biol* **1558**:271-301.

Pratt D, Chen J, Pillich R, Rynkov V, Gary A, Demchak B and Ideker T (2017) NDEx 2.0: A Clearinghouse for Research on Cancer Pathways. *Cancer Res* **77**:e58-e61.

Pratt D, Chen J, Welker D, Rivas R, Pillich R, Rynkov V, Ono K, Miello C, Hicks L, Szalma S, Stojmirovic A, Dobrin R, Braxenthaler M, Kuentzer J, Demchak B and Ideker T (2015) NDEx, the Network Data Exchange. *Cell Syst* **1**:302-305.

Reina S, Guarino F, Magri A and De Pinto V (2016) VDAC3 As a Potential Marker of Mitochondrial Status Is Involved in Cancer and Pathology. *Front Oncol* **6**:264.

Rostovtseva T and Colombini M (1996) ATP flux is controlled by a voltage-gated channel from the mitochondrial outer membrane. *J Biol Chem* **271**:28006-28008.

Schellenberg B, Wang P, Keeble JA, Rodriguez-Enriquez R, Walker S, Owens TW, Foster F, Tanianis-Hughes J, Brennan K, Streuli CH and Gilmore AP (2013) Bax exists in a

Downloaded from jpet.aspetjournals.org at ASPET Journals on April 20, 2024

JPET Fast Forward. Published on June 16, 2020 as DOI: 10.1124/jpet.120.000009
This article has not been copyedited and formatted. The final version may differ from this version.

dynamic equilibrium between the cytosol and mitochondria to control apoptotic priming. *Mol Cell* **49**:959-971.

Shannon P, Markiel A, Ozier O, Baliga NS, Wang JT, Ramage D, Amin N, Schwikowski B and Ideker T (2003) Cytoscape: a software environment for integrated models of biomolecular interaction networks. *Genome Res* **13**:2498-2504.

Shimizu S, Narita M and Tsujimoto Y (1999) Bcl-2 family proteins regulate the release of apoptogenic cytochrome c by the mitochondrial channel VDAC. *Nature* **399**:483-487.

Suttner DM and Dennery PA (1999) Reversal of HO-1 related cytoprotection with increased expression is due to reactive iron. *FASEB J* **13**:1800-1809.

Tajeddine N, Galluzzi L, Kepp O, Hangen E, Morselli E, Senovilla L, Araujo N, Pinna G, Larochette N, Zamzami N, Modjtahedi N, Harel-Bellan A and Kroemer G (2008) Hierarchical involvement of Bak, VDAC1 and Bax in cisplatin-induced cell death. *Oncogene* **27**:4221-4232.

Tang HL, Le AH and Lung HL (2006) The increase in mitochondrial association with actin precedes Bax translocation in apoptosis. *Biochem J* **396**:1-5.

Tomasello F, Messina A, Lartigue L, Schembri L, Medina C, Reina S, Thoraval D, Crouzet M, Ichas F, De Pinto V and De Giorgi F (2009) Outer membrane VDAC1 controls permeability transition of the inner mitochondrial membrane in cellulo during stress-induced apoptosis. *Cell Res* **19**:1363-1376.

Tsujimoto Y and Shimizu S (2000) VDAC regulation by the Bcl-2 family of proteins. *Cell Death Differ* **7**:1174-1181.

Vianello A, Casolo V, Petrussa E, Peresson C, Patui S, Bertolini A, Passamonti S, Braidot E and

Downloaded from jpet.aspetjournals.org at ASPET Journals on April 20, 2024

JPET Fast Forward. Published on June 16, 2020 as DOI: 10.1124/jpet.120.000009
This article has not been copyedited and formatted. The final version may differ from this version.

Zancani M (2012) The mitochondrial permeability transition pore (PTP) - an example of multiple molecular exaptation? *Biochim Biophys Acta* **1817**:2072-2086.

Wang Z, Lu W, Li Y and Tang B (2013) Alpinetin promotes Bax translocation, induces apoptosis through the mitochondrial pathway and arrests human gastric cancer cells at the G2/M phase. *Mol Med Rep* **7**:915-920.

Wettmarshausen J and Perocchi F (2017) Isolation of Functional Mitochondria from Cultured Cells and Mouse Tissues. *Methods Mol Biol* **1567**:15-32.

Xu T, Ding W, Ji X, Ao X, Liu Y, Yu W and Wang J (2019) Molecular mechanisms of ferroptosis and its role in cancer therapy. *J Cell Mol Med* **23**:4900-4912.

Yagoda N, von Rechenberg M, Zaganjor E, Bauer AJ, Yang WS, Fridman DJ, Wolpaw AJ, Smukste I, Peltier JM, Boniface JJ, Smith R, Lessnick SL, Sahasrabudhe S and Stockwell BR (2007) RAS-RAF-MEK-dependent oxidative cell death involving voltage-dependent anion channels. *Nature* **447**:864-868.

Youle RJ and Strasser A (2008) The BCL-2 protein family: opposing activities that mediate cell death. *Nat Rev Mol Cell Biol* **9**:47-59.

Yuan S, Fu Y, Wang X, Shi H, Huang Y, Song X, Li L, Song N and Luo Y (2008) Voltage-dependent anion channel 1 is involved in endostatin-induced endothelial cell apoptosis. *FASEB J* **22**:2809-2820.

Zaid H, Abu-Hamad S, Israelson A, Nathan I and Shoshan-Barmatz V (2005) The voltage-dependent anion channel-1 modulates apoptotic cell death. *Cell Death Differ* **12**:751-760.

Zhang H, Zhou L, Davies KJA and Forman HJ (2019a) Silencing Bach1 alters aging-related

Downloaded from jpet.aspetjournals.org at ASPET Journals on April 20, 2024

JPET Fast Forward. Published on June 16, 2020 as DOI: 10.1124/jpet.120.000009
This article has not been copyedited and formatted. The final version may differ from this version.

changes in the expression of Nrf2-regulated genes in primary human bronchial epithelial cells. *Arch Biochem Biophys* **672**:108074.

Zhang L, Zhang J, Ye Z, Manevich Y, Ball LE, Bethard JR, Jiang YL, Broome AM, Dalton AC, Wang GY, Townsend DM and Tew KD (2019b) Isoflavone ME-344 Disrupts Redox Homeostasis and Mitochondrial Function by Targeting Heme Oxygenase 1. *Cancer Res* **79**:4072-4085.

Zhang L, Zhang J, Ye Z, Townsend DM and Tew KD (2019c) Pharmacology of ME-344, a novel cytotoxic isoflavone. *Adv Cancer Res* **142**:187-207.

Zoratti M and Szabo I (1994) Electrophysiology of the inner mitochondrial membrane. *J Bioenerg Biomembr* **26**:543-553.

Zoratti M, Szabo I and De Marchi U (2005) Mitochondrial permeability transitions: how many doors to the house? *Biochim Biophys Acta* **1706**:40-52.

Downloaded from jpet.aspetjournals.org at ASPET Journals on April 20, 2024

JPET Fast Forward. Published on June 16, 2020 as DOI: 10.1124/jpet.120.000009
This article has not been copyedited and formatted. The final version may differ from this version.

Footnotes

Funding

This work was supported by grants from the National Institutes of Health (5P20GM103542-09 - COBRE in Oxidants, Redox Balance and Stress Signaling) and support from the South Carolina Centers of Excellence program and was conducted in a facility constructed with the support from the National Institutes of Health, Grant Number C06 RR015455 from the Extramural Research Facilities Program of the National Center for Research Resources.

Downloaded from jpet.aspetjournals.org at ASPET Journals on April 20, 2024

JPET Fast Forward. Published on June 16, 2020 as DOI: 10.1124/jpet.120.000009
This article has not been copyedited and formatted. The final version may differ from this version.

Figure legends

Figure 1. VDAC 1 and 2 were identified as ME-344 targets in H460 cells by using click-chemistry and mass spectrometry. Affinity-enriched and gel-fractionated proteins between 10-250 kDa were analyzed by LC/MS-MS and quantified by label free proteomics. **A.** Proteins with a $\log_2$ fold change in intensity >2.5 were considered enriched with M2F as compared to control beads. **B.** Twelve proteins enriched with M2F were queried for known protein interactions revealing VDAC 1 and 2 interactions with 5 of the other enriched proteins. This network of interactions was visualized with Cytoscape. **C.** Functional annotations for VDAC1 and 2 extracted from the Reactome and KEGG databases.

Figure 2. Manipulation of VDAC 1/2 expression impacts drug response. A. Expression of VDAC isoforms VDAC1, VDAC2 and VDAC3 in H460 and H596 cell lines were determined by qPCR. **B.C.** After transfection, mRNA and protein expression of the corresponding VDAC isoforms were assessed by qPCR and western blot. **D.E.** After transfection, H460 and H596 cell lines were treated with ME-344 (0-100 μM) for 24 h and viabilities determined by trypan blue assay where % viability was calculated relative to non-target control. **F.H.** Basal intracellular ROS levels determined with CM-H_2DCFDA by flow cytometry. **G.I.** Statistical analyses of cell ROS levels. Data are derived from three independent experiments and presented as means ± SD in the scatter plots. *$p < 0.05$, ***$p < 0.001$ vs. the untreated control by Student's t-test.

Downloaded from jpet.aspetjournals.org at ASPET Journals on April 20, 2024

JPET Fast Forward. Published on June 16, 2020 as DOI: 10.1124/jpet.120.000009
This article has not been copyedited and formatted. The final version may differ from this version.

Figure 3. Manipulation of VDAC 1/2 expression impacts ROS production. A-D. Cells were treated with their IC_{50}s of ME-344 for 24 hours and intracellular ROS levels determined with CM-H_2DCFDA by flow cytometry. **E-H.** Statistical analyses of cell ROS levels. Data are derived from three independent experiments and presented as means ± SD in the scatter plots. *$p < 0.05$, **$p < 0.01$ vs. the untreated control by Student's t-test.

Figure 4. Impact of ME-344 on apoptosis. A.B. ME-344 treated cells were cultured for 24 h prior to staining with Annexin V and PI. **C.D.** Statistical analyses of cell apoptosis. Live: Annexin V and PI double negative cells. Apoptosis: Annexin V positive, PI positive or negative cells. Data are derived from three independent experiments and presented as means ± SD in the scatter plots. *$p < 0.05$, ***$p < 0.001$ vs. the untreated control by Student's t-test.

Figure 5. Manipulation of VDAC 1/2 expression impacts apoptosis. A-H. ME-344 treated (at their IC_{50}s: 10.05±0.28, 14.74±0.32, 13.81±0.23, 9.38±0.29 uM, respectively) VDAC knockdown-cells were cultured for 24 h prior to staining with Annexin V and PI. **I-L.** Statistical analyses of cell apoptosis. Live: Annexin V and PI double negative cells. Apoptosis: Annexin V positive, PI positive or negative cells. Data are derived from three independent experiments and presented as means ± SD in the scatter plots. **$p < 0.01$ vs. the untreated control by Student's t-test.

Figure 6. Impact of ME-344 on mitochondrial membrane potentials. Following ME-344, cells were cultured for 24 h prior to: **A.E.** Red images indicate JC-1

Downloaded from jpet.aspetjournals.org at ASPET Journals on April 20, 2024

JPET Fast Forward. Published on June 16, 2020 as DOI: 10.1124/jpet.120.000009
This article has not been copyedited and formatted. The final version may differ from this version.

aggregate fluorescence in healthy mitochondria, while green represent cytosolic JC-1 monomers. Merged images indicate co-localization of JC-1 aggregates and monomers. Scale bar = 10 μm. Images are representative of 3 independent experiments. **B.F.** MFI fold change quantification of JC-1 green/red ratio in control and ME-344 treatment groups. **C.G.** MMP loss assay by flow cytometry. The right lower region of dot plots for JC-1-stain represents JC-1 positive cells (green color). The right upper region represents JC-1 negative cells (red color). **D.H.** The percentage of JC-1 positive cell lines in control and ME-344 treatment groups. Data are derived from three independent experiments and presented as means ± SD in the scatter plots. **$p < 0.01$, ***$p < 0.001$ vs. the untreated control by Student's t-test.

Figure 7. ME-344 decreases mitochondrial membrane potential in drug sensitive cells. A.C. Representative images of TMRM staining on H460 (sensitive) and H596 (resistant) cells. Cells were treated with either DMSO or ME-344 and the same fields followed for 3 h. **B.D.** Quantification of mean intensity of TMRM fluorescence. Data normalized to baseline of DMSO (baseline = 1). **E.G.** ME-344 treated cells were cultured for different times prior to TMRM staining and MMP measured by flow cytometry. Representative results of TMRM staining; **F.H.** Statistical analysis of mitochondrial membrane potential. Data are derived from three independent experiments and presented as means ± SD in the scatter plots. *$p < 0.05$, **$p < 0.01$, ***$p < 0.001$ vs. the untreated control by Student's t-test.

Figure 8. VDAC knockdown decreases mitochondrial membrane potential and

Downloaded from jpet.aspetjournals.org at ASPET Journals on April 20, 2024

JPET Fast Forward. Published on June 16, 2020 as DOI: 10.1124/jpet.120.000009
This article has not been copyedited and formatted. The final version may differ from this version.

VDAC 1 and 2 knockdown induce recovery of mitochondrial membrane potential in sensitive cell line H460. A. Representative images of TMRM staining on post transfection H460 cells. Cells were treated with ME-344 and the same fields were followed for 1 h after treatment. **B.** Mean basal TMRM fluorescence after knockdown was plotted in comparison to transfection with non-target siRNA. **C.** Quantification is mean intensity of TMRM fluorescence. Data are normalized to baseline (baseline = 1). Data are derived from three independent experiments and presented as means ± SD in the scatter plots. *$p < 0.05$, **$p < 0.01$, ***$p < 0.001$ vs. the baseline control by Student's t-test.

Figure 9. VDAC 1 and 2 knockdown prevented ME-344-induced Bax translocation and cytochrome c release in sensitive cell line H460. A.C. H460 and H596 cells transfected with non-target or siVDAC1, 2, 3 were all treated with ME-344 and mitochondria and cytosol isolated. Proteins were separated by SDS-PAGE and evaluated by immunoblots. **B.D.** Protein expression after ME-344 was quantified by ImageJ software - in either mitochondrial or cytosol fractions relative to non-target control cells. β-actin as cytosol marker; ATP5A as mitochondria marker; SERCA as endoplasmic reticulum (ER) marker. Data are derived from three independent experiments and presented as means ± SD in the scatter plots. **$p < 0.01$, ***$p < 0.001$ vs. each control group by Student's t-test.

Downloaded from jpet.aspetjournals.org at ASPET Journals on April 20, 2024

Figure 1

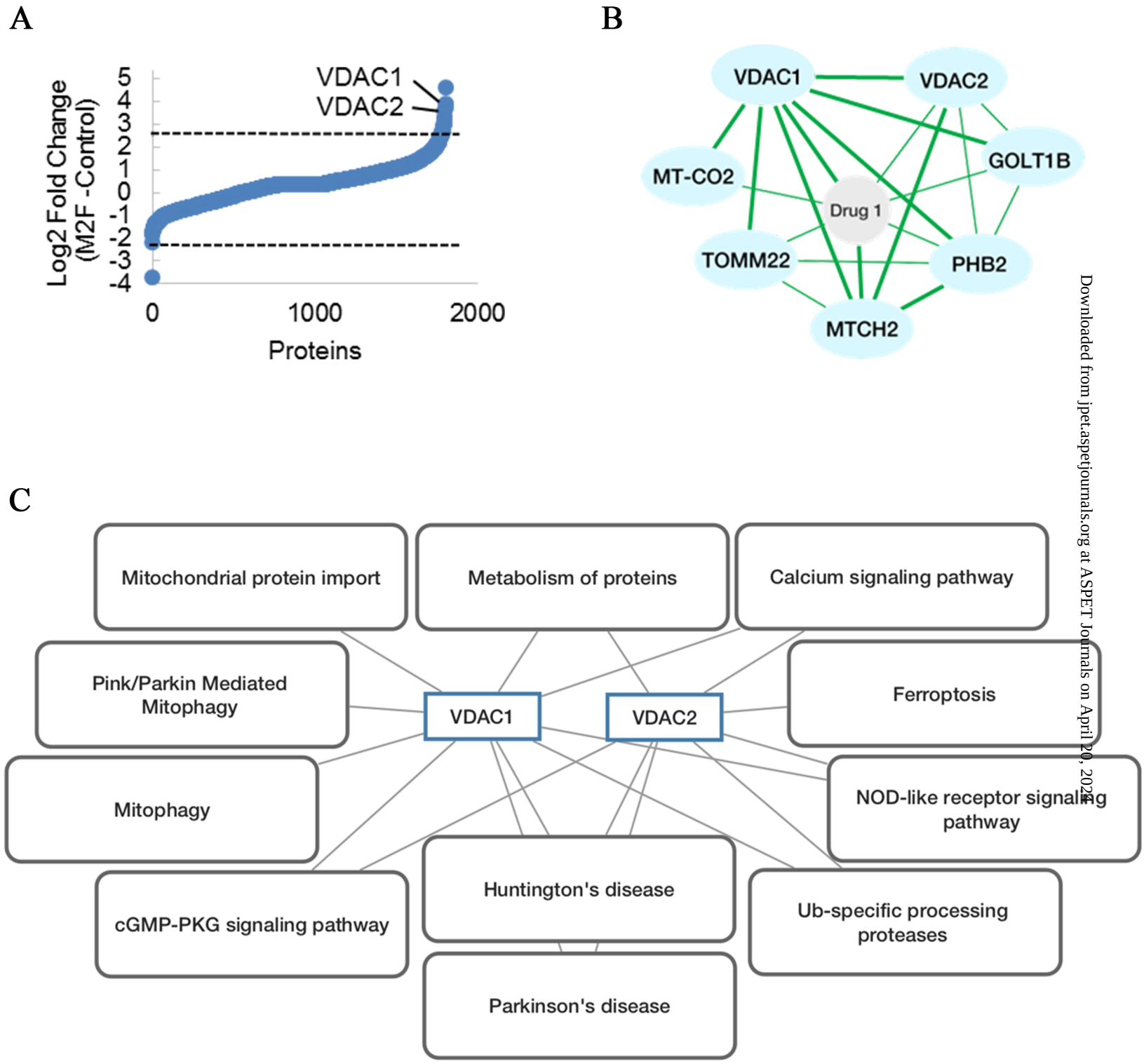

Downloaded from jpet.aspetjournals.org at ASPET Journals on April 20, 2024

Figure 2

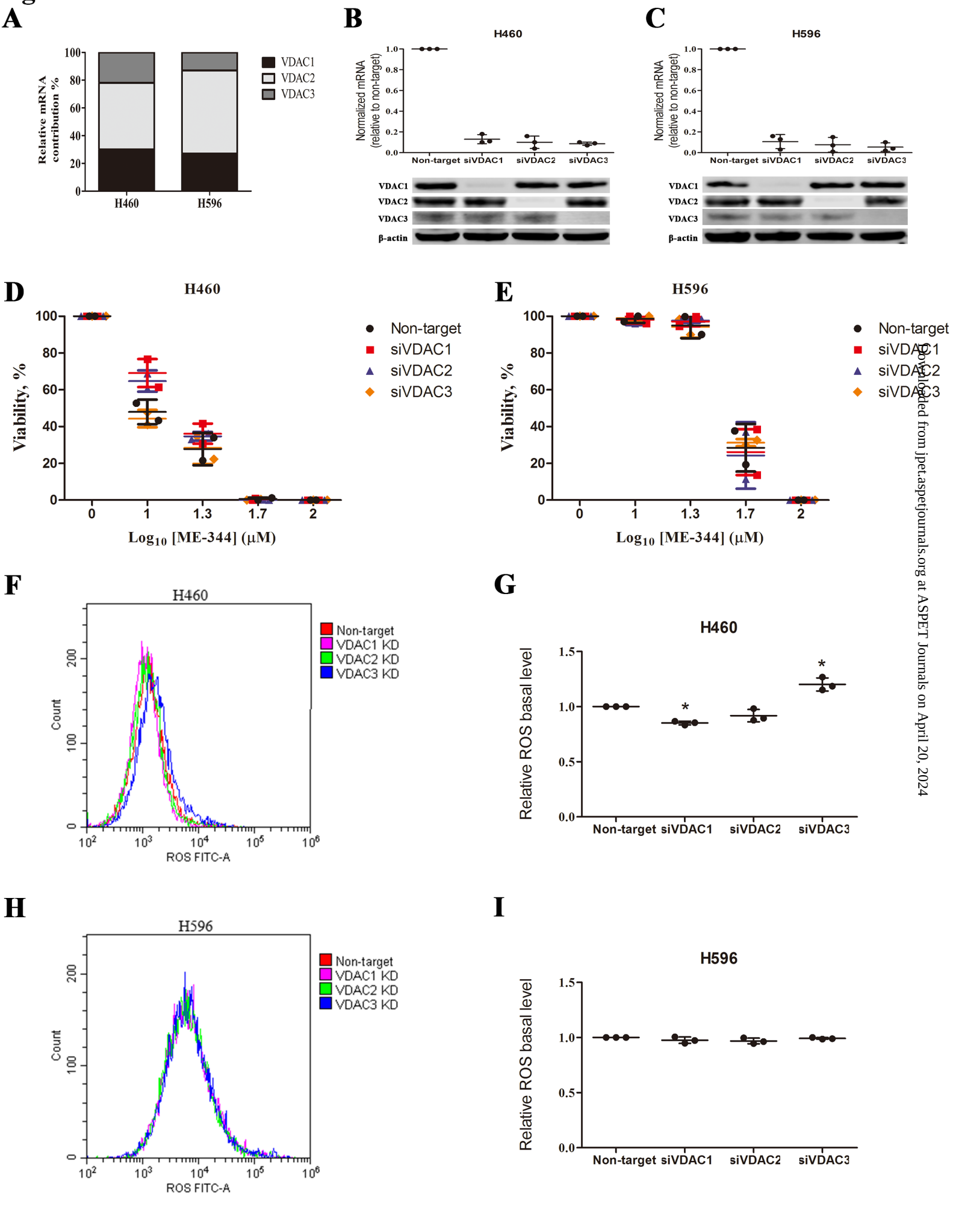

Downloaded from jpet.aspetjournals.org at ASPET Journals on April 20, 2024

Figure 3

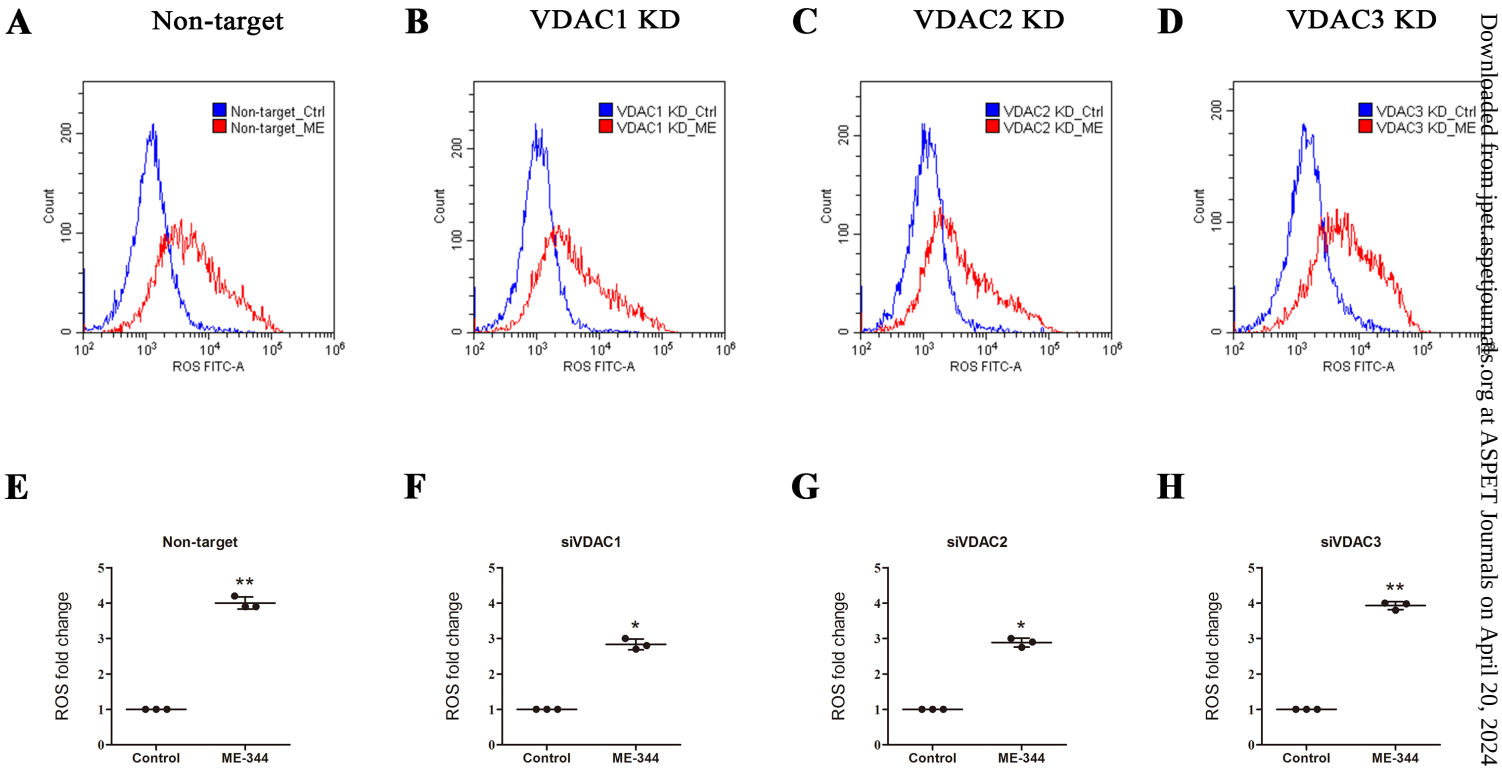

Downloaded from jpet.aspetjournals.org at ASPET Journals on April 20, 2024

Figure 4

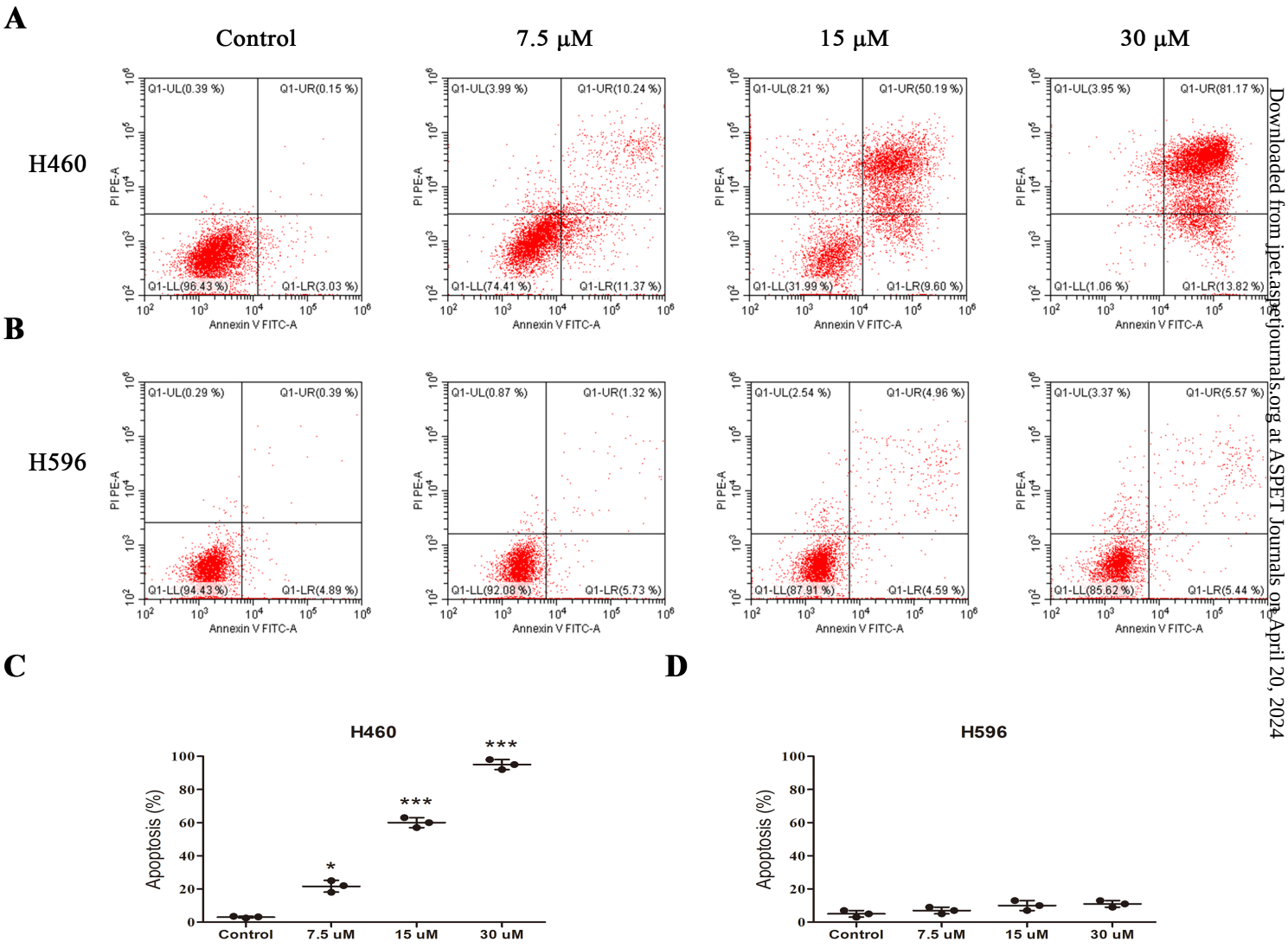

Downloaded from jpet.aspetjournals.org at ASPET Journals on April 20, 2024

Figure 5

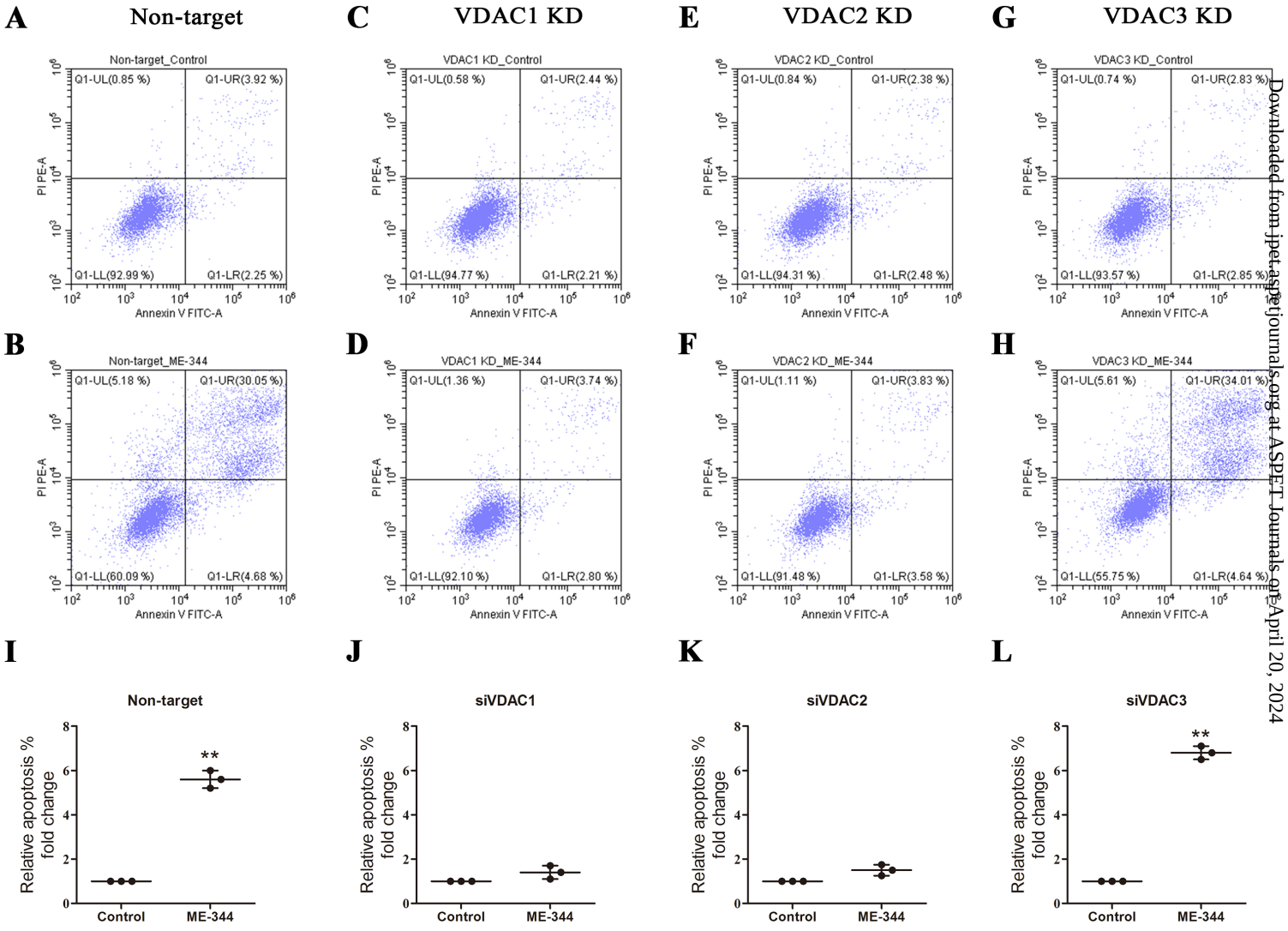

Downloaded from jpet.aspetjournals.org at ASPET Journals on April 20, 2024

Figure 6

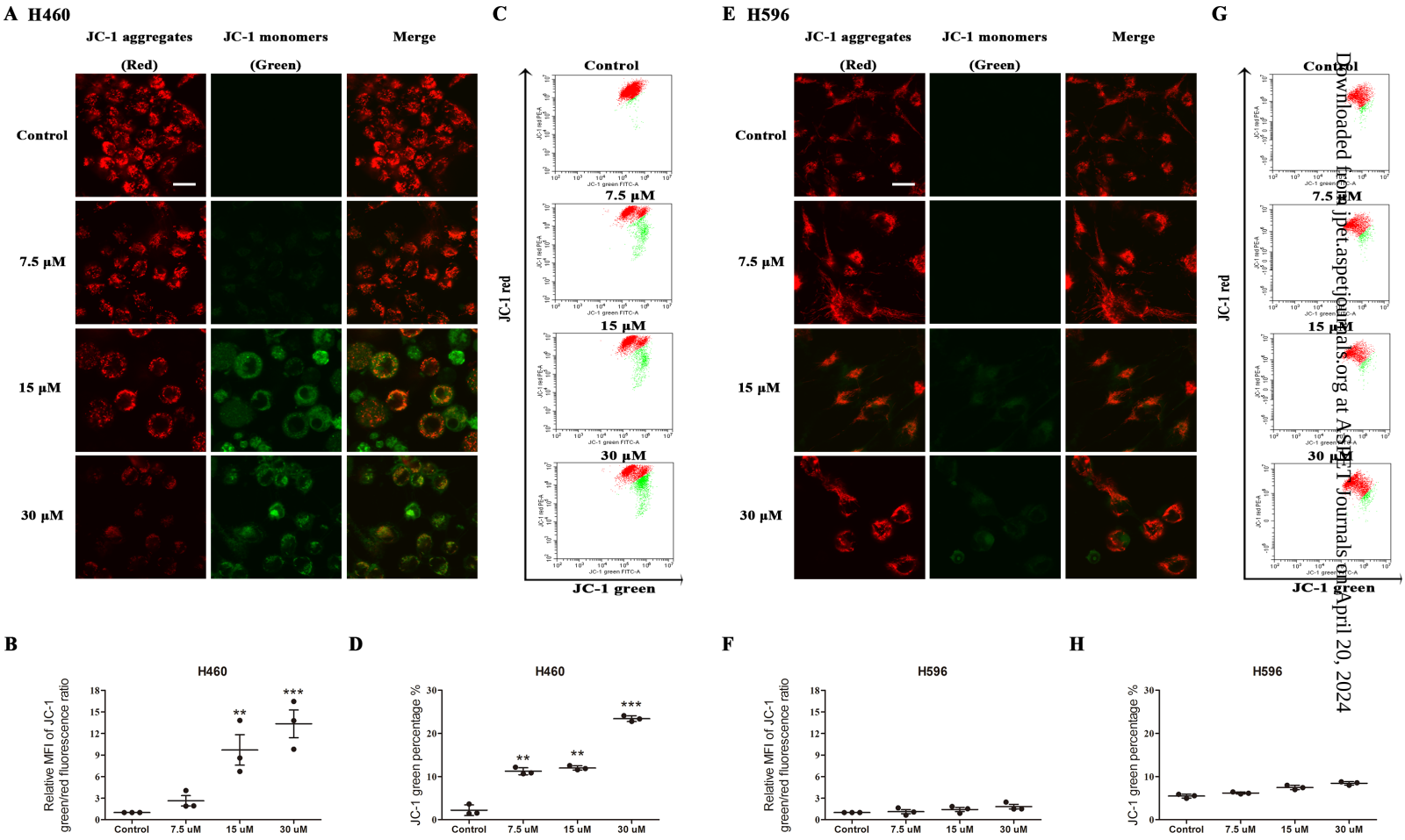

Downloaded from jpet.aspetjournals.org at ASPET Journals on April 20, 2024

Figure 7

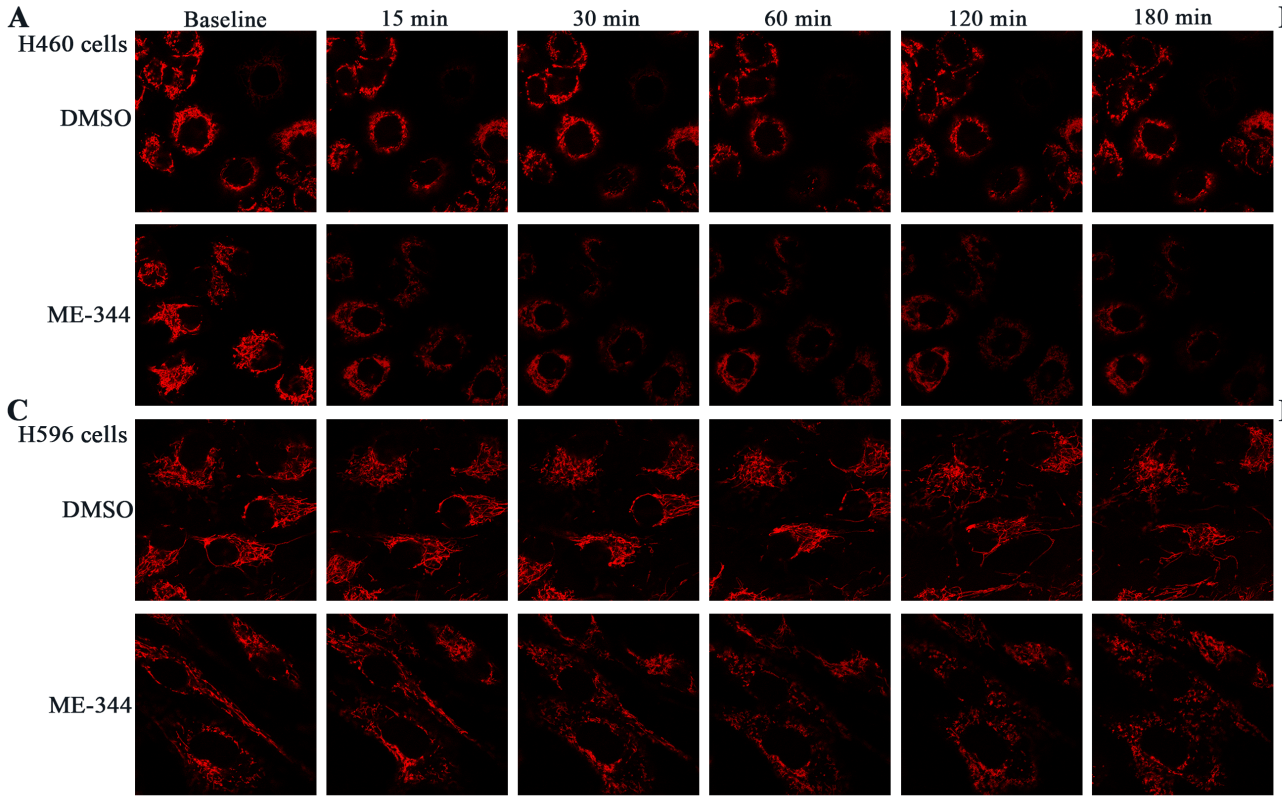

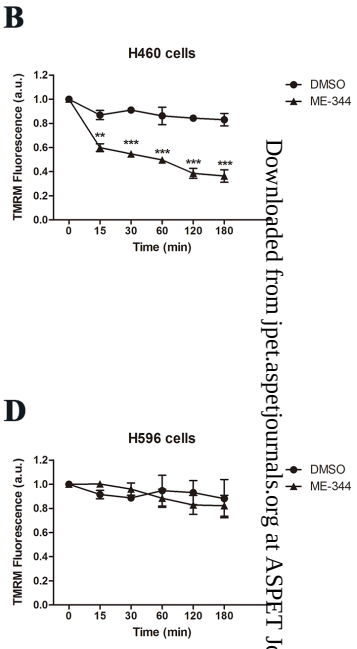

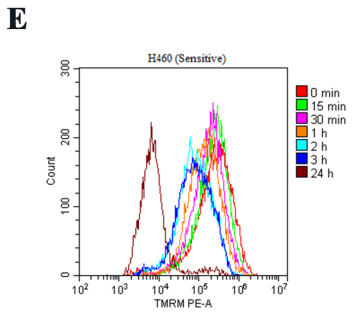

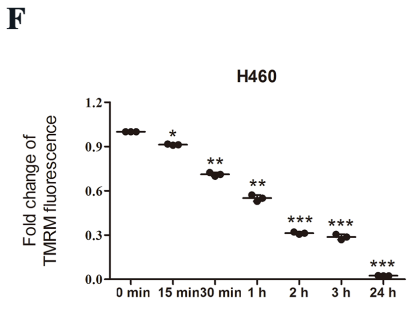

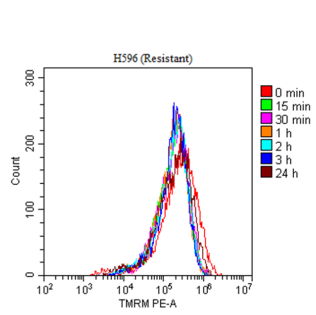

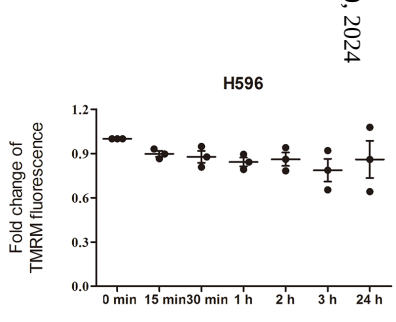

Downloaded from jpet.aspetjournals.org at ASPET Journals on April 20, 2024

Figure 8

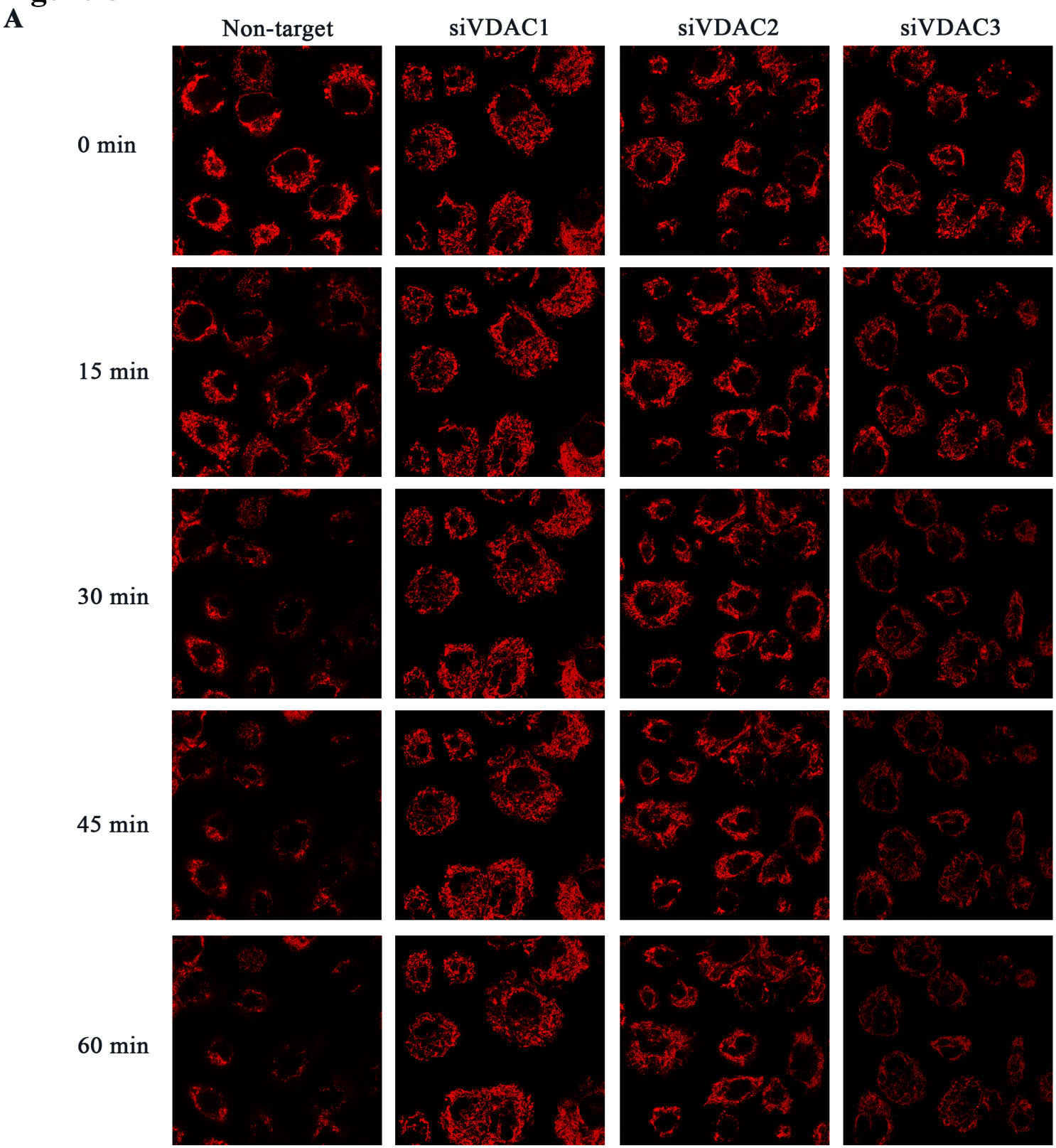

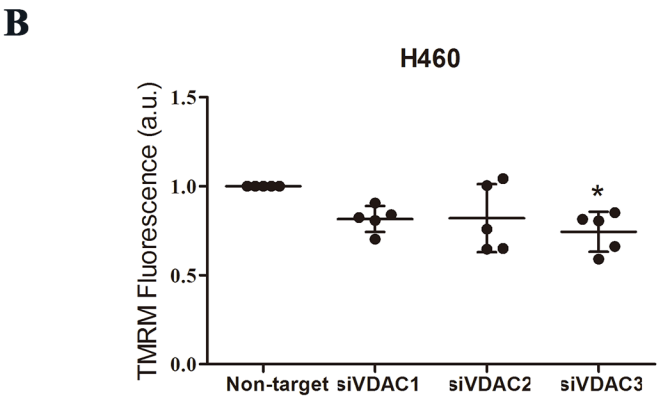

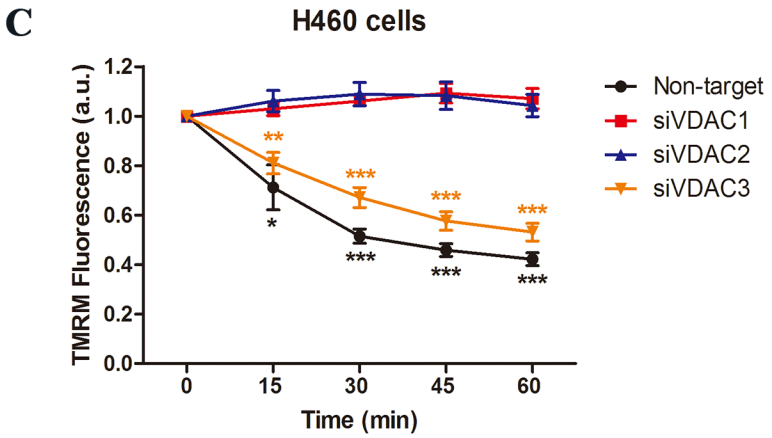

Downloaded from jpet.aspetjournals.org at ASPET Journals on April 20, 2024

Figure 9

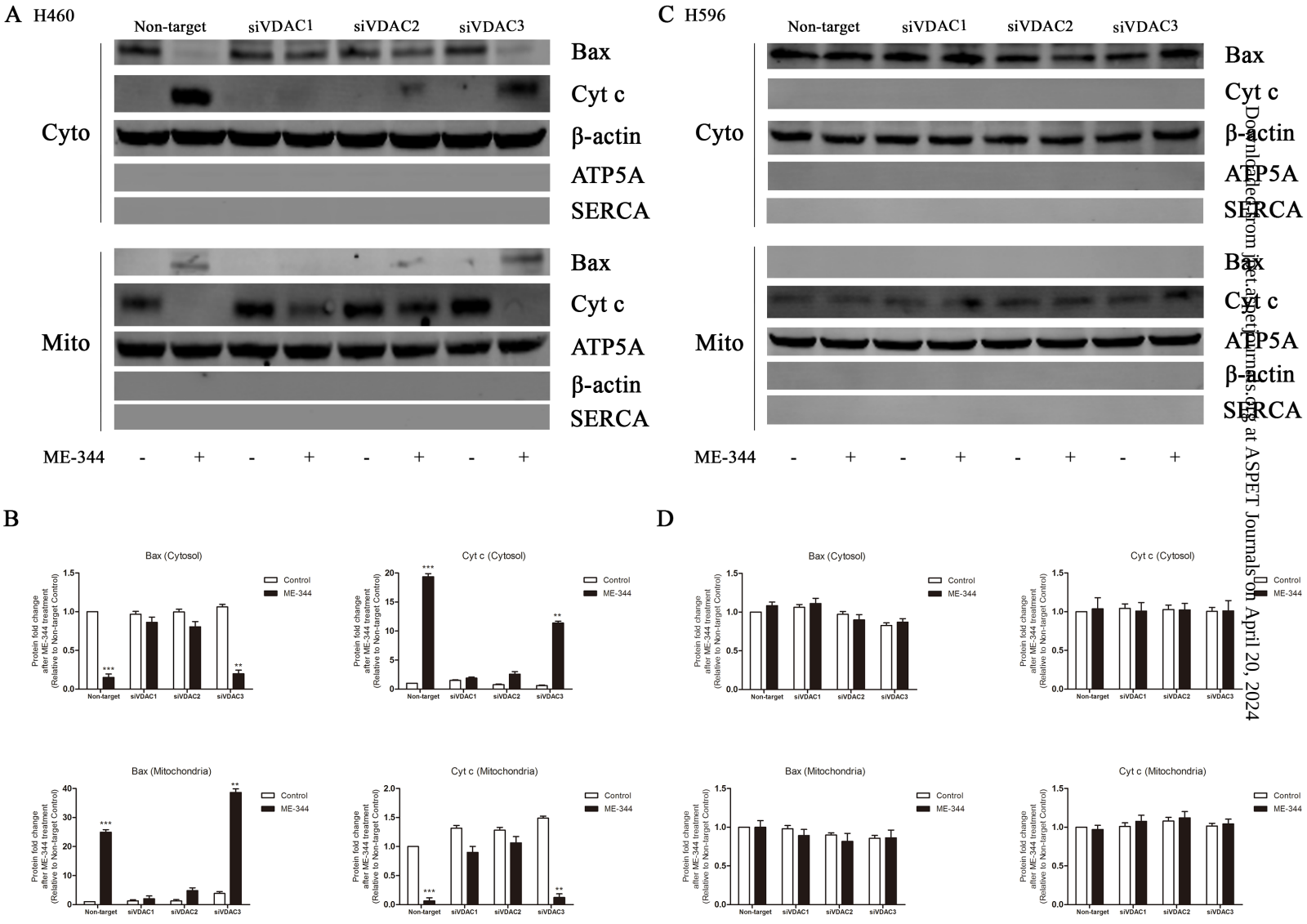

Downloaded from jpet.aspetjournals.org at ASPET Journals on April 20, 2024